The Application of Hilbert–Huang Transforms to Meteorological Datasets

DEAN G. DUFFY

NASA Goddard Space Flight Center, Greenbelt, Maryland

(Manuscript received 14 May 2003, in final form 28 October 2003)

ABSTRACT

Recently a new spectral technique has been developed for the analysis of aperiodic signals from nonlinear systems—the Hilbert–Huang transform. It is shown how this transform can be used to discover synoptic and climatic features: For sea level data, the transforms capture the oceanic tides as well as variations in precipitation patterns. In the case of solar radiation, variations in the diurnal and seasonal cycles are observed. Finally, from barographic data, the Hilbert–Huang transform reveals the passage of extratropical cyclones, fronts, and troughs. Thus, this technique can detect signals on synoptic to interannual time scales.

1. Introduction

For generations researchers have used Fourier analysis to analyze signals. Because both the signal and its Fourier transform are important in understanding most processes, contour plots of the signal energy as functions of time and frequency (temporal–frequency analysis) have the potential of painting a more revealing picture than just the temporal signal or frequency analysis alone.

The earliest time–frequency representation (TFR) was the short-time Fourier transform (STFT; see Allen and Rabiner 1977). This scheme divides the temporal signal $f(t)$ into a series of small overlapping pieces. Each piece is then windowed and individually Fourier transformed. The STFT of a function $f(t)$ is defined by

$$F_{\mathrm{ST}}(t, \omega) = \frac{1}{2\pi} \int_{-\infty}^{\infty} f(t) h(t - \tau) e^{-i\omega\tau}\, d\tau, \qquad (1)$$

where $h(\tau)$ is the window function. Contour plots of the energy density function $|F_{\mathrm{ST}}(t, \omega)|$ are typically presented. This scheme is most useful when the physical process is linear, so that the superposition of sinusoidal solutions is valid and the time series is *locally* stationary, so that the Fourier coefficients are slowly changing.

One of the drawbacks of STFT is the presence of a fixed window, although Czerwinski and Jones (1997) have developed a short-time Fourier analysis with an adaptively adjusting window. Wavelet analysis (see Daubechies 1992; Torrence and Compo 1998) seeks to address this defect by decomposing the time series into *local*, time-dilated, and time-translated wavelet components using time–frequency atoms or wavelets ψ. The wavelet transform of the signal $f(t)$ is then

$$F_{\mathrm{WT}}(a, b) = \frac{1}{\sqrt{a}} \int_{-\infty}^{\infty} f(t) \psi\left(\frac{t - b}{a}\right) dt, \qquad (2)$$

where a is the scale and b is the time shift. The wavelet transform represents the energy in the signal of temporal scale a at $t = b$. Wavelet analysis is attractive because 1) it is local, although higher frequencies are more localized; 2) it has uniform temporal resolution for all frequency scales; and 3) it is useful for characterizing gradual frequency changes. However, it is nonadaptive because the same basic wavelet is used for all data.

Finally, empirical orthogonal function (EOF) analysis or its Fourier transform version, the singular spectral analysis (SSA), decomposes a time series using eigenfunctions of the covariance matrix (see Ghil et al. 2002). This analysis is quite different from the short-time Fourier transform or wavelet analyses because the EOFs are derived from data. However, its distribution of eigenvalues does not yield characteristic time or frequency scales. Furthermore, the eigenfunctions themselves are not necessarily linear or stationary and therefore are not easily analyzed by spectral modes.

From our experience with short-time Fourier transforms, wavelets, and EOF analyses, an ideal scheme for the spectral analysis of signals would be complete (i.e., the sum of the modes equals the original signal), orthogonal, local, and adaptive. This method would also allow us to extract local time and frequency scales. The Hilbert–Huang transform is another step toward this goal.

Hilbert transforms were originally developed to solve integral equations. Instead of re-expressing a function of time with its Fourier transform that depends on fre-

Corresponding author address: Dr. Dean G. Duffy, Code 912, NASA Goddard Space Flight Center, Greenbelt, MD 20771.
E-mail: duffy@agnes.gsfc.nasa.gov

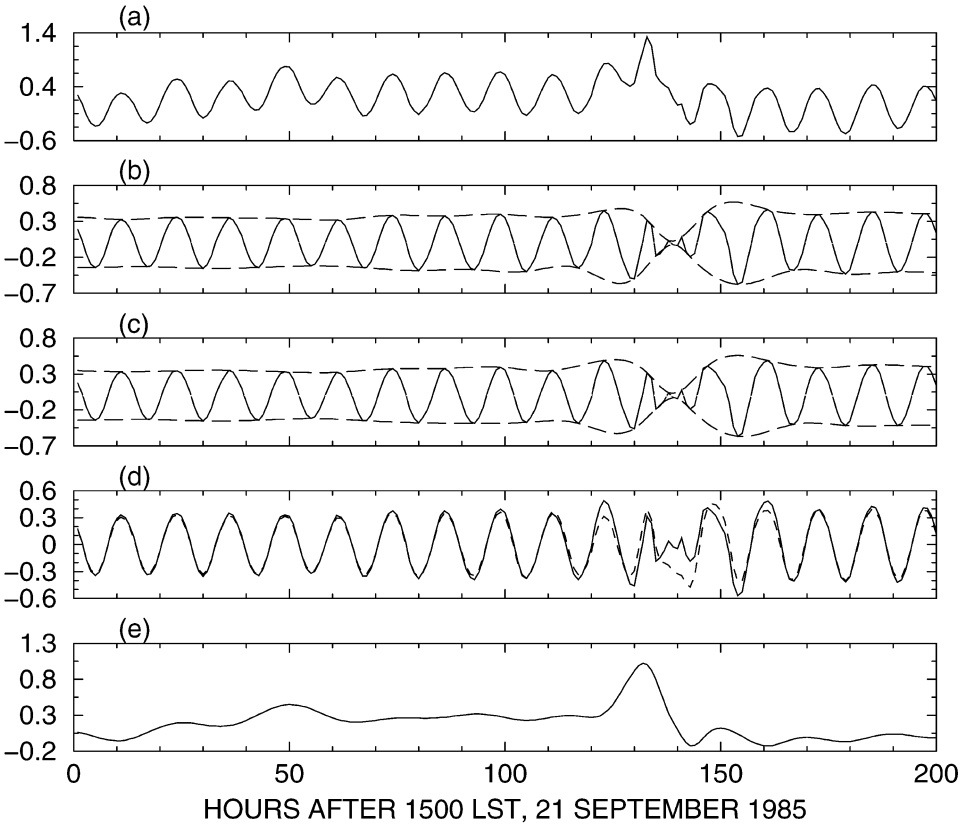

FIG. 1. The computation of the first intrinsic mode function from a sea level dataset. The solid line in (a) shows a portion of the original data with sea level height (in m). The solid lines in (b) and (c) show the first intrinsic mode when the mode's extrema and zero crossings are equal or differ by one for the first and third times, respectively. The dashed lines give the envelopes, while the dotted line is the mean. (d) The first IMF from the original dataset (solid line) and the original data after applying a Shapiro filter (dashed line). (e) The signal after the first intrinsic mode has been removed.

quency, the Hilbert transform yields another temporal function that has been phase shifted by $-90°$ via the integral definition:

$$\hat{f}(t) = \frac{1}{\pi} \int_{-\infty}^{\infty} \frac{f(\tau)}{t - \tau}\, d\tau. \tag{3}$$

By itself, this holds little interest for us. However, when Gabor (1946) developed his theory of communications Hilbert transforms appeared in his concept of *analytic signal*, $z(t) = f(t) + i\hat{f}(t)$. A particularly interesting case occurs if $f(t)$ is band limited. Then we can rewrite $z(t) \approx A(t)e^{i\theta(t)}$, a local time-varying wave with amplitude $A(t)$ and phase $\theta(t)$.

Most signals are not band limited. Huang's great contribution was to devise a method, which he calls *sifting*, that decomposes a wide class of signals into a set of band-limited functions, which he calls *intrinsic mode functions* (IMFs). In their original paper, Huang et al. (1998a) tested out their analysis on simple nonlinear systems such as Stokes waves and the solutions to the Duffing and Lorenz equations. Subsequently, the Hilbert–Huang analysis has been applied to signals from pulmonary blood pressure (Huang et al. 1998b) to earthquake signals (Huang et al. 2001) to the rotational residuals from the solar convection zone (Komm et al. 2001). In the atmospheric sciences, these transforms have been applied to climatic signals (Pan et al. 2003; Salisbury and Wimbush 2002; Wu et al. 1999; Xie et al. 2002). The purpose of this paper is to illustrate the advantages of applying Hilbert–Huang transforms to signals that include synoptic as well as climatic signals.

A detailed description of the scheme is provided in section 2. In section 3, this scheme is then applied to datasets of sea level heights, incoming solar radiation, and barographic data. Conclusions are presented in section 4.

2. Procedure

The process of developing time–frequency diagrams using Hilbert–Huang transforms consists of three steps.

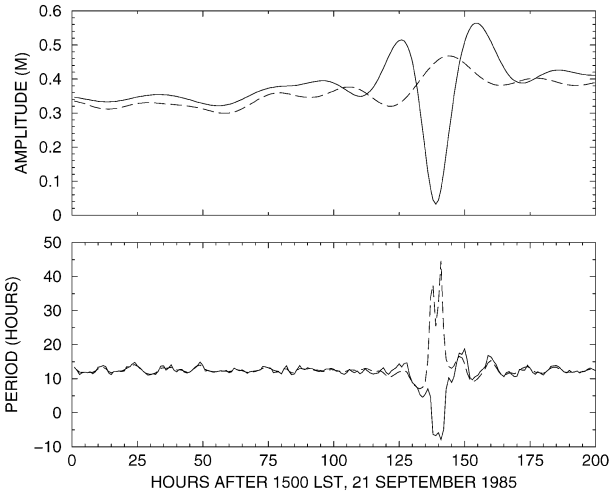

FIG. 2. The solid line gives the amplitude and period of the first IMF shown in Fig. 1. The dashed line also gives the amplitude and period of the first IMF of the signal shown in Fig. 1 but the data have first been Shapiro filtered.

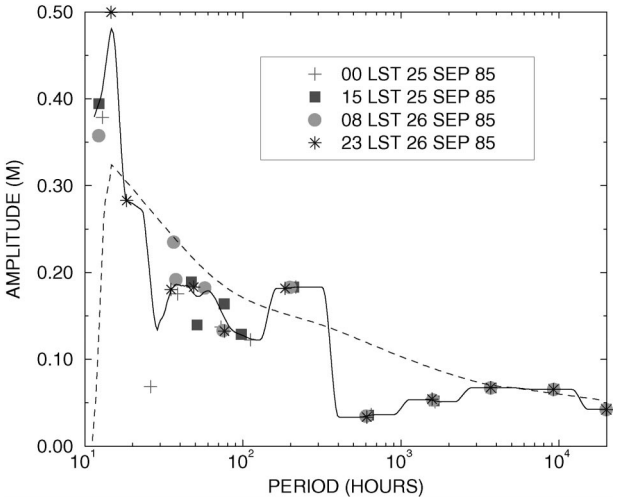

FIG. 3. Using sea level data, the curve fit when instantaneous amplitudes and periods over a 24-h interval are grouped together to form a single Hilbert–Huang transform (solid line). The dotted line is the average of 24 curve fits to each hour's instantaneous amplitudes and periods. Some of the instantaneous amplitudes used in computing the averages are plotted as data points.

The first step decomposes or ''sifts'' the signal into its intrinsic mode functions. The first intrinsic mode gives the smallest *local* variations of the original signal. Using a cubic spline, two envelope curves are generated, one of which connects the maxima of the signal while the other connects the minima. From these curves the mean is computed. The difference between the signal and this mean constitutes a first guess of the first IMF. If the IMF were sinusoidal, then the number of extrema would equal the number of zero crossings, or differ by one. This is usually not the case and suggests that our first guess, while good, needs further refinement because there may be yet smaller scales buried in the data.

Originally Huang et al. [1998a, their Eq. (5.5)] repeated this sifting process until a Cauchy-like integral condition was satisfied. In later papers they adopted a stopping criterion based on the number extrema and zero crossings. When these quantities were equal, or differed by one, for three consecutive iterations, the IMF is set to the values found in the final iteration. This is the criterion that shall be used. Although it cannot be proven mathematically, this procedure always converged for the datasets tested here.

To illustrate the decomposition process, Fig. 1 presents various steps in computing the first IMF. Figure 1a presents a small portion of the original dataset—sea level observations taken at the mouth of the Chesapeake Bay during the 1980s. In addition to the oscillations due to the oceanic tides, there is a large peak at 133 h due to the passage of Hurricane Gloria during the early hours of 27 September 1985.

Figures 1b and 1c show the first IMF after it has satisfied the convergence criteria for the first and last (third) time, respectively. Also shown are the top and bottom envelopes (the dashed lines) as well as the mean (the dotted line). Note how the sifting process has generated a mode that is symmetrical with respect to the abscissa.

It will be shown shortly that this first IMF represents the semidiurnal tides. This mode varies smoothly except in the interval 125–150 h. If the original data record in Fig. 1a is examined this behavior can be associated with several ''kinks'' in the data record. It is unclear whether these kinks are real or due to a failure of the instrument.

To examine the effects that such kinks have on the construction of the IMFs, smooth the original data with a single pass of a simple Shapiro filter [a digital filter

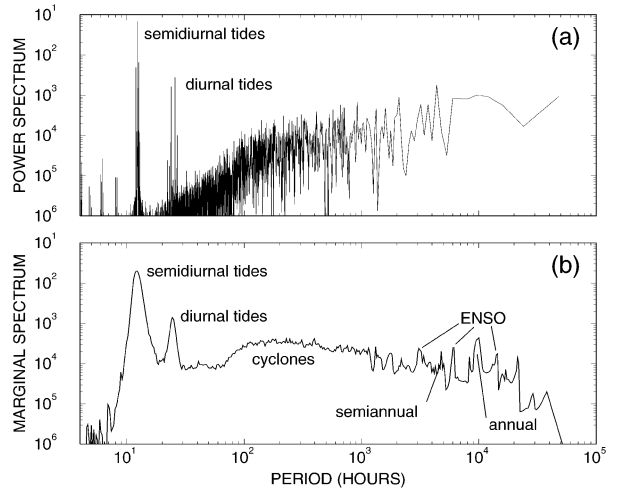

FIG. 4. The (a) Fourier power spectrum and (b) average marginal spectrum (in m^2) derived from 48 000 h of sea level observations at the mouth of the Chesapeake Bay.

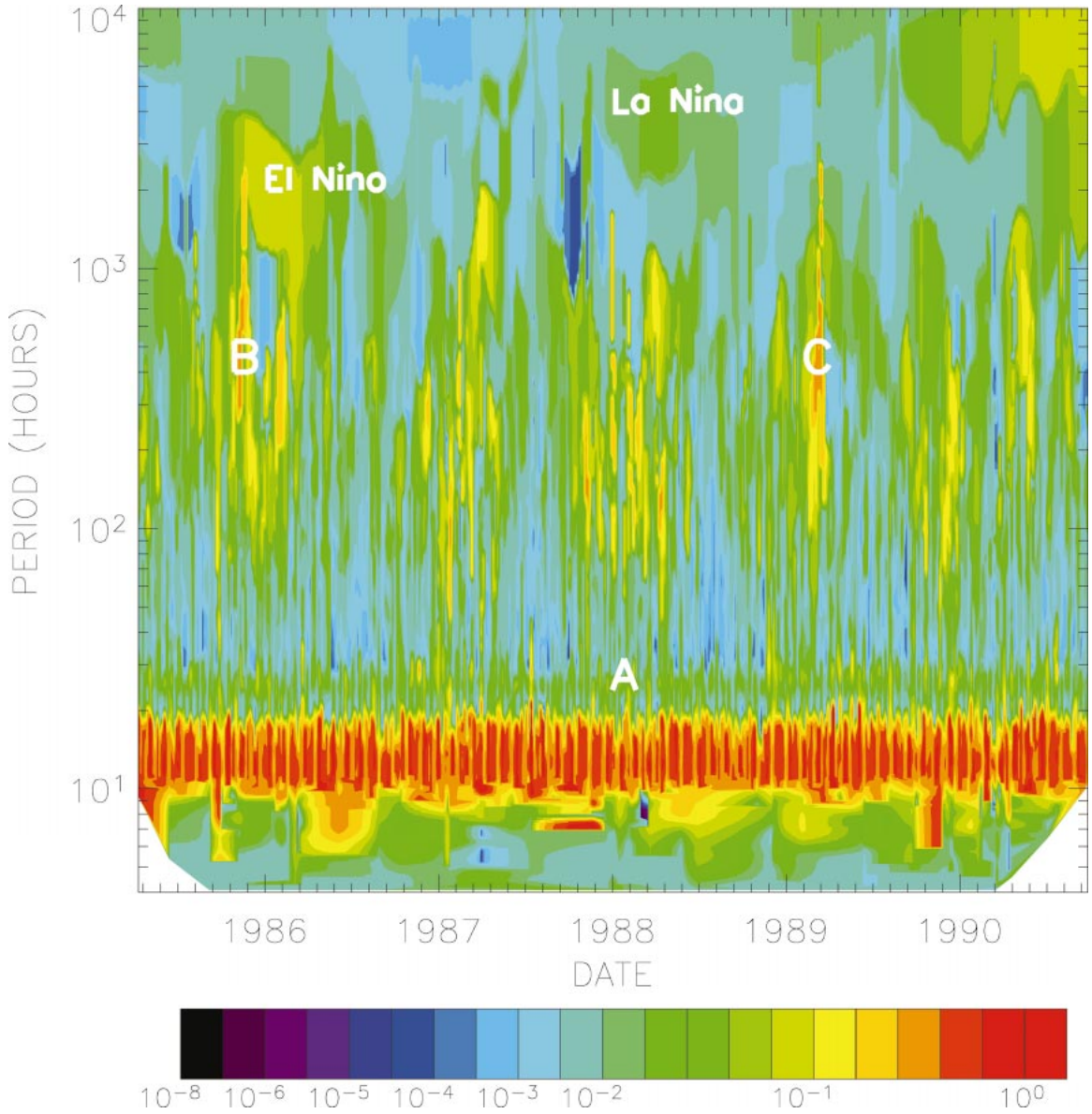

FIG. 5. Contour plot of the Hilbert spectrum of the sea level heights (in m^2) at the mouth of the Chesapeake Bay as a function of time and period. The amplitudes were time averaged, as described in the text, over 480 h.

developed by Shapiro (1970) that eliminates waves with a period of $2\Delta t$ but leaves longer-period waves relatively unaffected]. After sifting, Fig. 1d gives the first IMF of the original (solid line) and smoothed (dashed line) data. This improved behavior in the structure of the IMF might argue for smoothing the data before applying Hilbert–Huang transforms. Unfortunately, filtering is a two-edged sword: It both modifies the true signal and eliminates noise. Because Huang–Hilbert transforms were designed specifically to analyze aperiodic and nonlinear signals (signals from nonlinear systems), the use of a linear filter could alter the signal in ways that might compromise the usefulness of the technique. For this reason, the presence of the noise will simply be endured.

Once the first IMF is found, it is subtracted from the signal, yielding a residual that is smoother and has a lower frequency than the original signal because the first IMF captures the smallest local variation of the signal (see Fig. 1e). The process then begins anew with the residual to obtain the second IMF.

Having found the second IMF, it is subtracted from the residual, leaving an even smoother residual. Further modes are found in the same manner, and the sifting process concludes when there is no longer any maxima

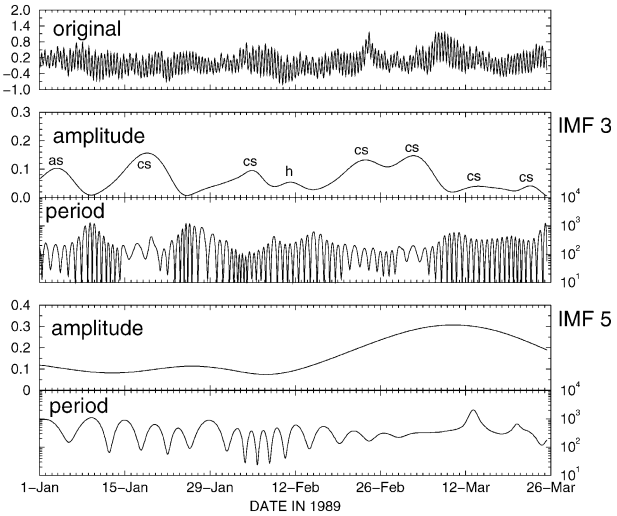

FIG. 6. A portion of third and fifth IMFs from the Hilbert–Huang analysis of 48 000 h of sea level heights taken at the mouth of the Chesapeake Bay. For the IMFs, the scale for the amplitudes (in m) is given on the left while the period (in h) is given on the right.

or minima in the residual. The original signal equals the sum of the various IMFs plus this small residual trend.

One drawback in using a cubic spline to obtain the envelope curve is the possibility of large swings near the endpoints. The method of Komm et al. (2001), that adds buffer zones on each end that equal the length of the original data, has been adopted. The signal was extrapolated into these buffer zones by fitting a sine wave using the closest extrema and zero crossing to define the frequency and amplitude of the wave.

Having determined the IMFs, the second step consists of computing the Hilbert transform $\hat{f}(t)$ of each mode $f(t)$ and then the corresponding analytic signal $z(t) = f(t) + i\hat{f}(t)$. Because only numerical values are available, the conventional method of computing $\hat{f}(t)$ is to take the fast Fourier transform of the data, multiply the transform by $i\,\mathrm{sgn}(\omega)$, and then take the inverse Fourier transform of this product (see Čížek 1970 or Henrici 1986, p. 203). Here sgn( ) denotes the sign function.

Computing the instantaneous frequency $\omega(t)$ from the data is difficult because it is the time derivative of $\theta(t)$. Barnes (1992) tested a number of methods to compute it from $f(t)$ and $\hat{f}(t)$. He found that the best representation of the instantaneous frequency is

$$\omega(t) = \frac{1}{2\Delta t}\tan^{-1}\left[\frac{f(t-\Delta t)\hat{f}(t+\Delta t) - f(t+\Delta t)\hat{f}(t-\Delta t)}{f(t-\Delta t)f(t+\Delta t) + \hat{f}(t+\Delta t)\hat{f}(t-\Delta t)}\right], \tag{4}$$

where Δt denotes the time between observations. This is the method that will be used.

Figure 2 illustrates the instantaneous amplitude $A(t)$ and period $P(t) = 2\pi/\omega(t)$ corresponding to the first IMF shown in Fig. 1. The solid and dashed lines give the results for the original signal and Shapiro-filtered signal, respectively. In both cases, the period equals approximately 12.5 h outside of the region from 125 to 150 h. Within the interval there are considerable differences between the orginal and smoothed data. Because analytic signals cannot have negative frequencies, the appearance of some suggests that the data are not correct here. For this reason, we will discard any amplitudes and periods when they are negative. This is acceptable because when the frequencies are negative the amplitude is small, as Fig. 2 shows.

Once the analytic signal for each IMF is obtained, the final task remains to display the results graphically. Although $A(t)$ and $P(t)$ could be plotted for each IMF, a better idea is to plot the square of the amplitude as a function of $P(t)$ and time, combining amplitude and period measurements of all IMF components on a single figure. This contour plot is commonly called the Hilbert spectrum, $H(t, \omega)$. Although two IMFs can have the same period, this will not occur at the same time and there is no ambiguity in constructing the Hilbert spectrum. Because most geophysical datasets contain a mixture of phenomena, with time scales varying from hours to years, it was found convenient to work with the logarithm of the instantaneous period rather than the period itself.

One problem with displaying the results is the irregularity of the location of the frequencies associated with each IMF at a given instant. Not only are these locations irregular but they also vary with time. Although most graphical packages can handle such irregularly spaced data, the plots are too noisy. One possible solution would be to construct a smoothed field before plotting.

If the instantaneous amplitudes are viewed as ''data'' observed at various instantaneous periods, then regression techniques developed by statisticians for fitting a curve through data can be used (Ryan 1997, chapter 10). Because there is little a priori knowledge about the shape of the curve, a nonparametric scheme that includes a kernel smoother is used. [Such a scheme was developed by Herrmann (1996); the FORTRAN 77 code is available online at http://www.unizh.ch/biostat/Software/kernf77.html.]

For large datasets, this method was modified to include time averaging. There are two possible methods. One method would group all of the instantaneous amplitudes and periods within a particular time interval

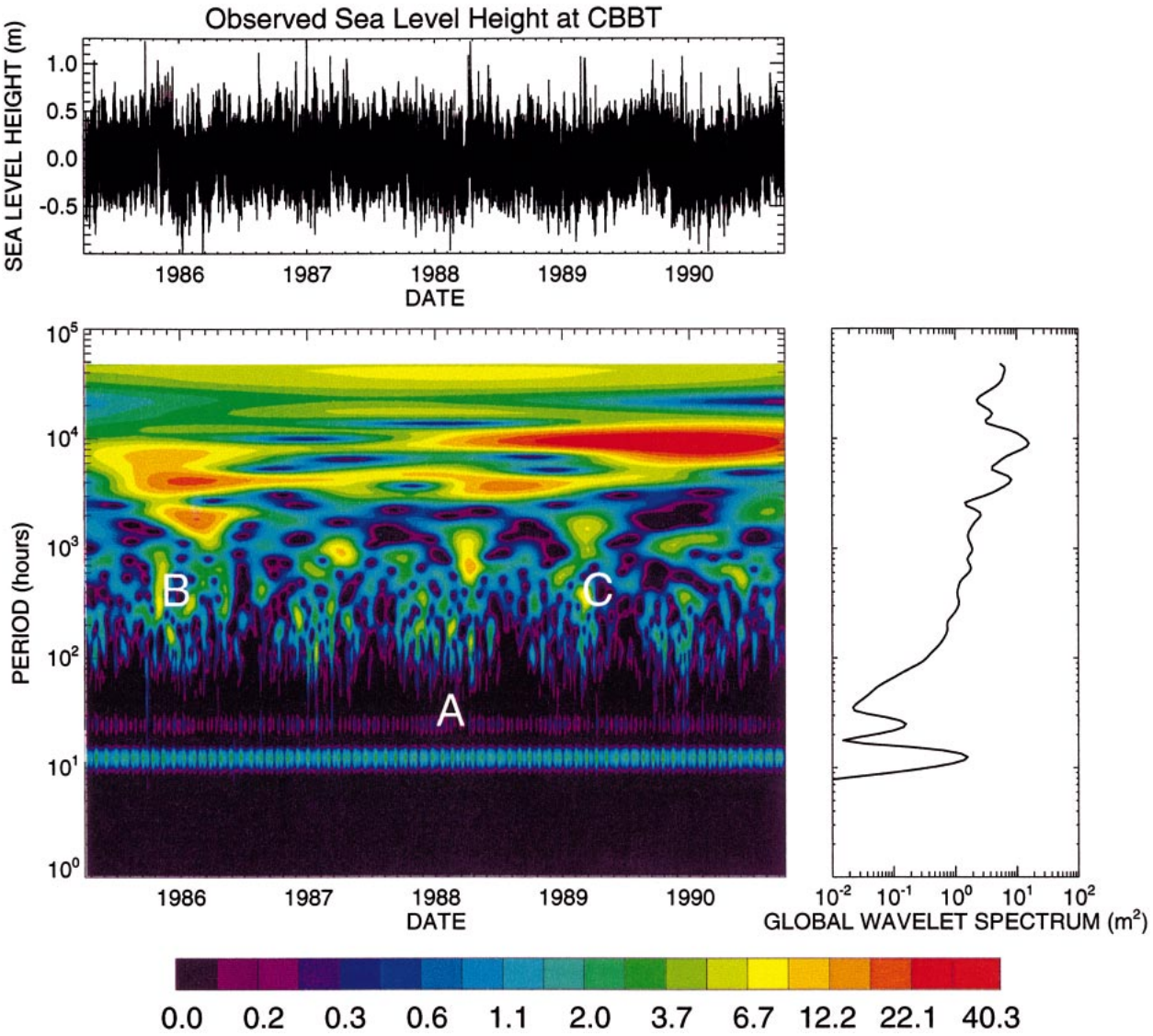

FIG. 7. Morlet wavelet analysis of sea level heights at the mouth of the Chesapeake Bay. The letter A denotes the diurnal tides, while B and C denote the Election Day Flood of Nov 1985 and the Feb 1989 snowstorm, respectively.

and assign them a common time. The second method would find curve fits at each time and then these curves would be averaged over an appropriate time interval. Figure 3 shows the instantaneous amplitudes and periods at four instances during the 24-h interval from 2330 LST 24 September 1985 to 2330 LST 26 September 1985 using sea level data. The solid line shows the grouping of instantaneous amplitudes and phases to form a single time value, while the dashed line shows the averaging of the curve fits. The first method retains the character of the higher-temporal-resolution amplitudes better compared to the second method.

As will be seen shortly, time–frequency plots contain a wealth of detail. For that reason, it is useful to integrate $H(t, \omega)$ over time, say from 0 to T. Because this *marginal spectrum* represents the energy of the signal, it is analogous to the power spectrum in Fourier analysis. Here a monochromatic, linear, and periodic signal appears as a sharp peak in the marginal spectrum, whereas a nonlinear and nonperiodic phenomenon yields a broad peak in the spectrum. If the marginal spectrum is normalized by T, we have the *average marginal spectrum.*

3. Applications

Having presented the procedure for constructing a Hilbert–Huang transform, this technique is now applied to three very different data fields: sea level heights, incoming solar radiation, and barographic observations.

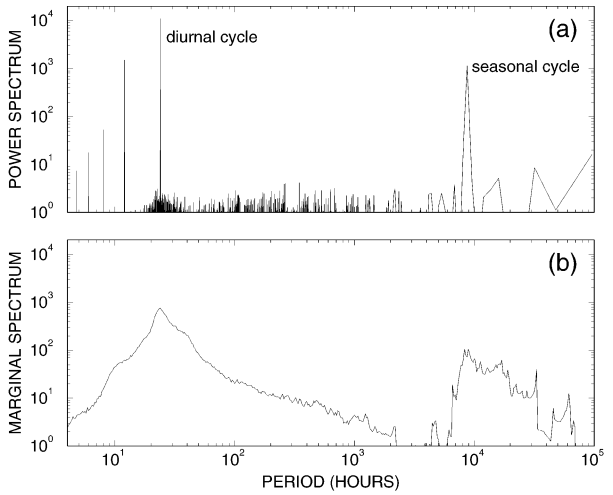

FIG. 8. The (a) Fourier power spectrum and (b) average marginal spectrum [in $(W\ m^{-2})^2$] derived from 96 000 h of diffuse solar radiation measured on a horizontal surface at ground level in Des Moines, IA.

a. Sea level heights

As a first application of the Hilbert–Huang transform to geophysical data, observations were obtained of the sea level heights observed at the Chesapeake Bay Bridge and Tunnel (CBBT) from 0000 LST 8 April 1984 to 2300 LST 28 September 1990. These 48 000 h of consecutive observations contain a wealth of physical phenomena—from highly predictable, astronomically forced tides to chaotic coastal storms.

Figure 4 shows the Fourier power spectrum and average marginal spectrum for the sea level heights. The Fourier analysis only reveals a semidiurnal tide with a period of 12.42 h and a diurnal tide with a period of 23.93 h. The average marginal spectrum also reveals the semidiurnal and diurnal tides. This is consistent with a study by Susanto et al. (2000), who showed that Hilbert–Huang transforms capture the diurnal and semidiurnal tides in the Makassar Straits. Furthermore, the marginal spectrum captures a wealth of other physical phenomena. For example, there is a peak near 100 h due to baroclinic instability. (Baroclinic instability is the instability of the prevailing atmospheric westerlies that generates cyclones. Its time scale is on the order of days.) At lower periods, we see peaks with annual and semiannual periods associated with the increased precipitation during the warmer months and the melting of snow during the spring. Finally, there are peaks associated with the intraseasonal event of the El Niño–Southern Oscillation (ENSO).

Figure 5 shows the Hilbert spectrum. A persistent maximum is found at approximately 12 h; this is the semidiurnal tides. A modulation in the amplitude that has a period of approximately 1 month is noted; this is the lunar forcing of the tides. There is also a faint green line at 24 h (denoted by the letter A), which is the diurnal tides.

At longer periods there are many local maxima. Two particularly large ones are highlighted in Fig. 5 by the letters B and C. Maximum B occurs during mid-November 1985 and is associated with the ''Election Day Flood,'' 4–7 November 1985, the second-worst river flood in Virginia during the twentieth century. During this event, heavy rain occurred in the mountainous regions of Virginia and West Virginia, and shown in Fig. 5 is the corresponding runoff.

February 1989 was the snowiest month (62 cm) in 50 yr (1948–99) for Norfolk, Virginia, due in large part to its heaviest 24-h snowfall (36 cm), which occurred during 17–18 February 1989. Point C in Fig. 5 corresponds to the melting and runoff of this snowpack during late February and early March 1989.

During the late 1980s, there were two significant ENSO events: an El Niño event in 1986 and a La Niña event in 1988. Because ENSO influences the precipitation and temperature along the U.S. East Coast, it is not surprising to see its signatures in the Hilbert spectrum.

The above analysis of Fig. 5 has shown that one of the possible uses of Hilbert–Huang transforms is the identification of significant events from the Hilbert spectrum. However, one might ask whether the original data could not simply be used. To answer this question, the original sea level data from the first 2000 h of 1989 have been plotted in Fig. 6. Also included are the third and fifth IMFs for the same period of time. By consulting daily weather maps, each peak in the third IMF's amplitude could be traced to the presence of cyclones in the North Atlantic (labelled as), coastal storms (cs), or a strong high pressure (h) located over New England, and its strong northerly winds. It would be very difficult to detect these phenomena in the original data. The large maximum in the fifth IMF's amplitude is due to the spring melt of the snowpack in the Appalachian Mountains.

As mentioned in the introduction, Hilbert–Huang transforms are one of several temporal–frequency techniques. A particularly popular one is wavelet analysis. Figure 7 shows the wavelet analysis [using an IDL package by Torrence and Compo (1998)] for our sea level height data. Clearly seen in the power spectrogram is the presence of the tides, storms (including the Election Day Flood and the 1989 snowstorm), and two ENSO events. The strong signal at $\sim 10^4$ h is from variations in the seasonal cycle. The primary difference is the smoothness of the spectrogram compared to the Hilbert spectrum.

In summary, the Hilbert–Huang transforms have discerned persistent, periodic features such as the tides, as well as episodic events such as snowmelt and heavy precipitation events.

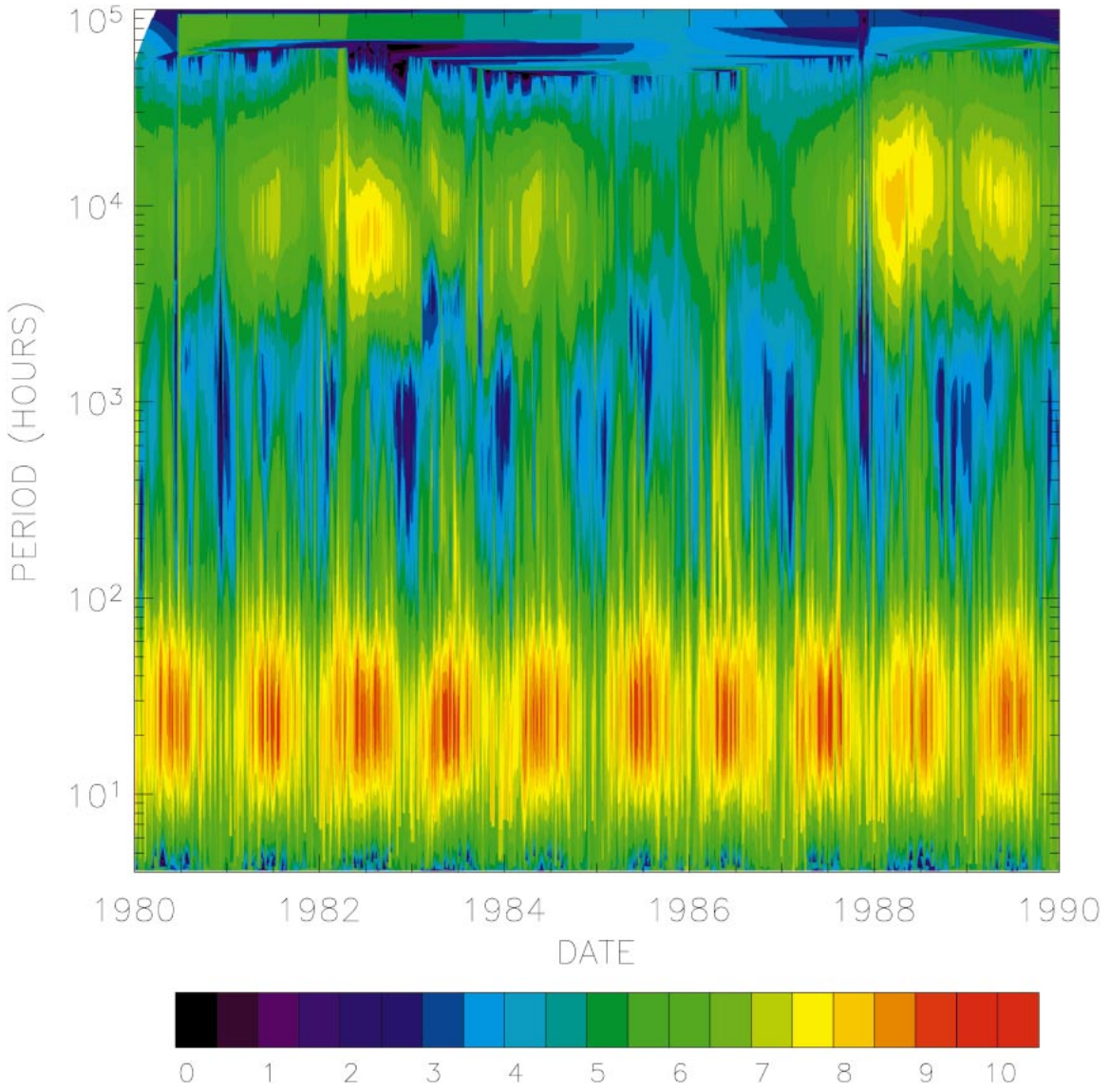

FIG. 9. Contour plot of the (natural) logarithm of the Hilbert spectrum of diffuse solar radiation [in $(W\ m^{-2})^2$] as a function of time and period. The amplitudes were time averaged, as described in the text, over 480 h.

b. Solar radiation

For the second dataset, the hourly diffuse horizontal radiation (the amount of solar radiation from the sky excluding the solar disk) for Des Moines, Iowa, from 1 January 1980 through 13 December 1990 is analyzed. (These observations may be found online at http://rredc.nrel.gov/solar/old_data/nsrdb/hourly.)

Figure 8 shows the Fourier power spectrum and average marginal spectrum. As one might expect, there are two peaks, one corresponding to the diurnal cycle and the other to the seasonal cycle.

Figure 9 shows the Hilbert spectrum for the signal. The maximum values occur along the line corresponding to a period of 24 h, the diurnal cycle, and during the summer months. For periods between 10^2 and 10^3 h, there are relative minima during the winter months due to the increased cloud cover that reduces the incoming radiation at ground level. Finally, for periods near 10^4 h the seasonal cycle is clearly seen. Of particular interest are the maxima that occur during 1982 and 1988. What physical phenomenon is the Hilbert–Huang transform detecting?

Recently, Koch and Mann (1996) studied the spatial and temporal variation of ^{7}Be, a natural radionuclide that is produced in the stratosphere and upper troposphere and is carried on aerosols. They found that ENSO events could significantly affect the concentration of this radionuclide. They suggested that this signal was due to observed rainfall anomalies during ENSO and its effect on the aerosol concentration in the troposphere.

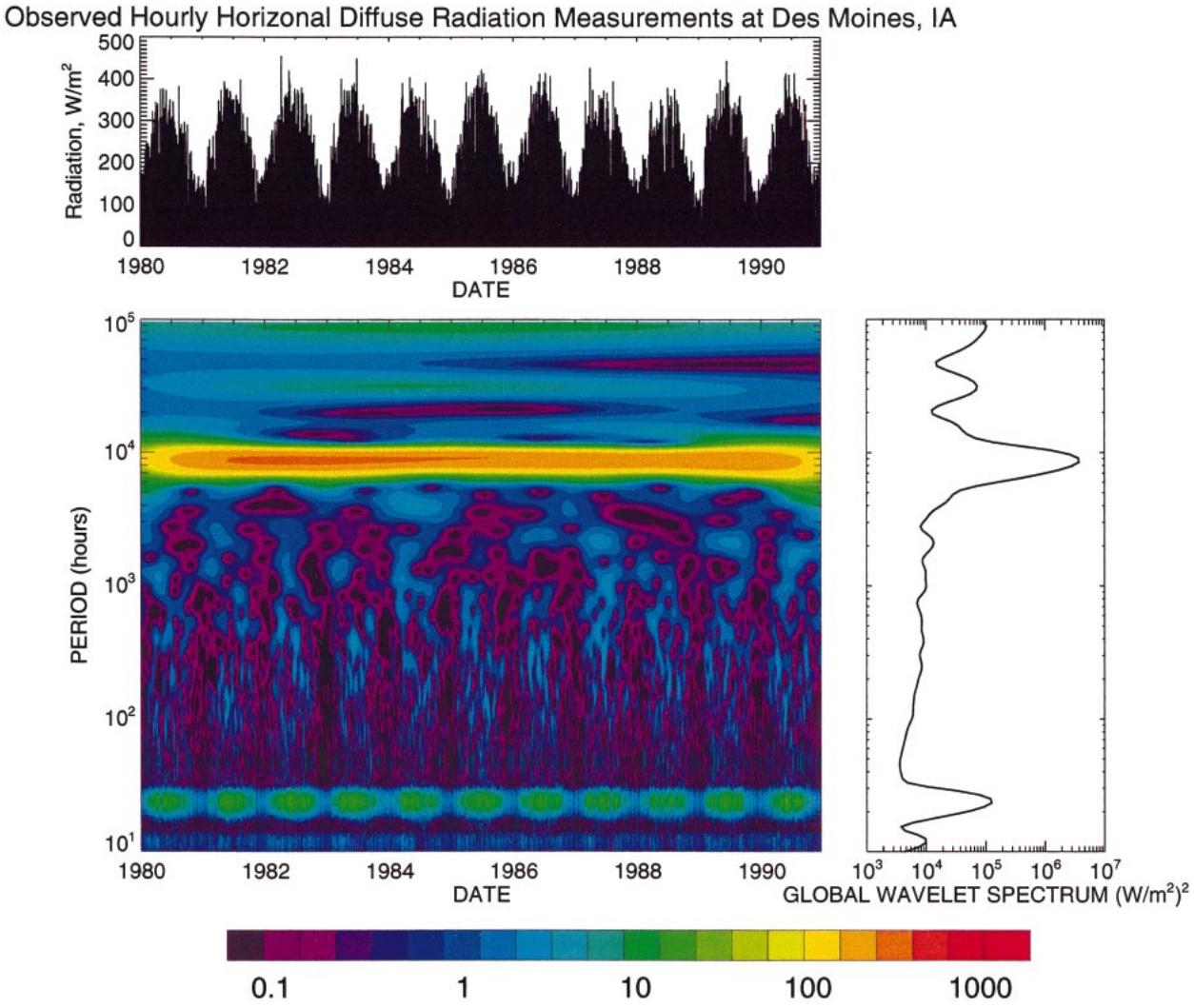

FIG. 10. Morlet wavelet analysis of diffuse solar radiation over Des Moines, IA, during the 1980s.

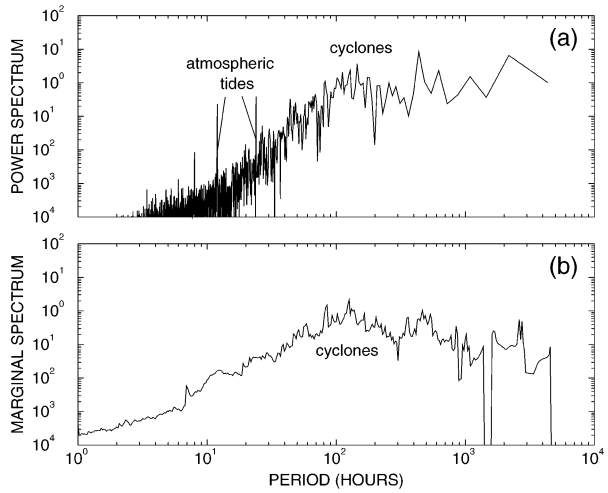

FIG. 11. The (a) Fourier power spectrum and (b) average marginal spectrum (in hPa^2) derived from barographic observations near Champaign–Urbana, IL, during the latter half of 1995.

Because the amount of sunlight scattered by aerosols depends on their concentration, our maxima correspond to the El Niño event of 1982, as well as the eruption of El Chichón, and the La Niña event of 1988. Apparently the El Niño event of 1986 did not significantly affect the aerosol concentration of Des Moines.

Finally, in Fig. 10, the wavelet analysis of the solar data is presented. It captures the diurnal and seasonal cycle (the signal at $\sim 10^4$ h) and the El Niño event of 1982. However, there is no maxima for either the 1986 or 1988 ENSO events, and the spectrogram is much smoother than the Hilbert–Huang analysis.

c. Barographic observations

Our third test involves barographic data averaged to produce observations at 2-min intervals from a network located in central Illinois (Grivet-Talocia et al. 1999). These data were grouped by station and quarter of the year.

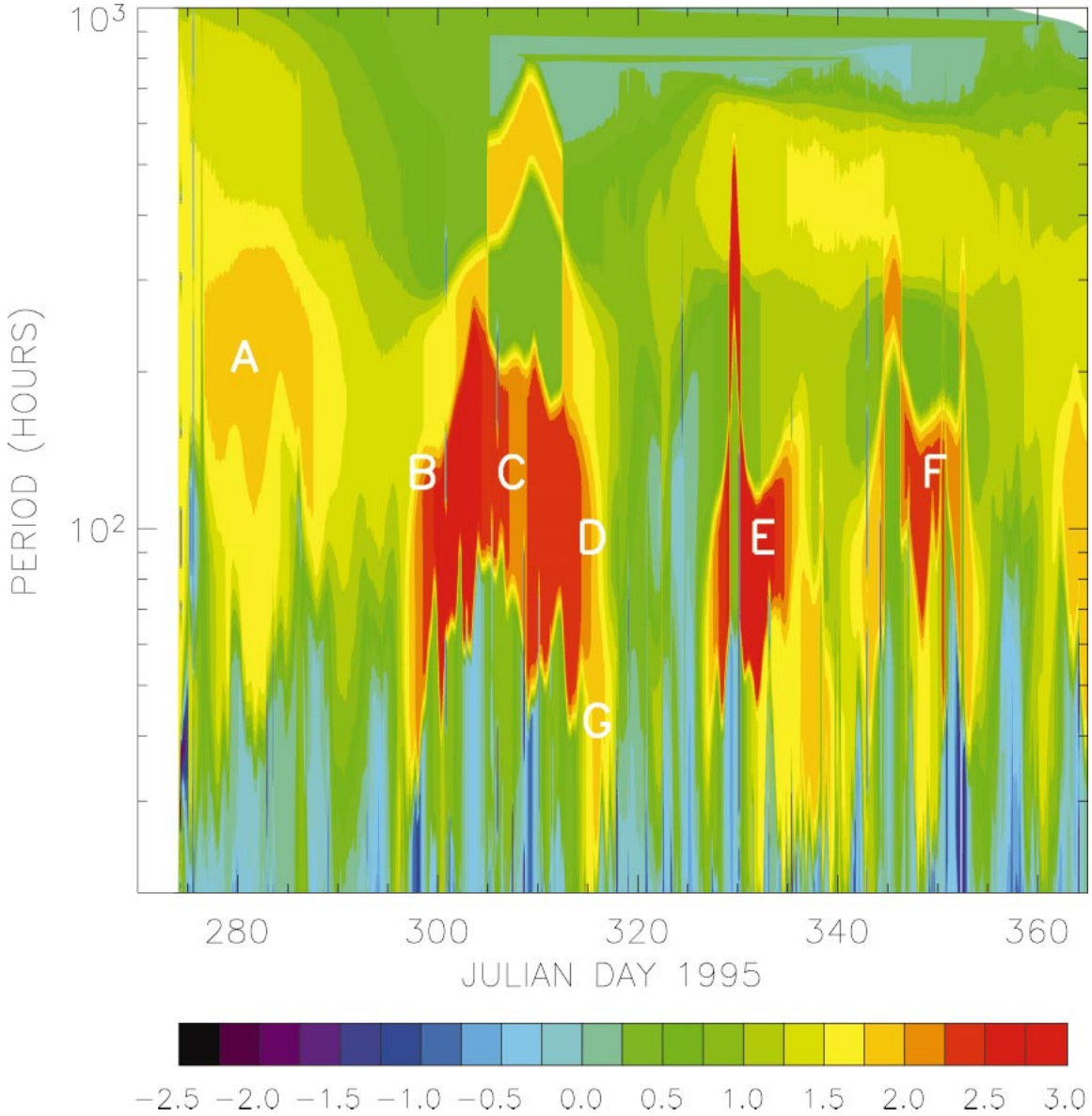

FIG. 12. Contour plot of the (natural) logarithm of the Hilbert spectrum of surface pressure (in hPa^2) as a function of time and period. The amplitudes were time averaged, as described in the text, over 128 min.

Figure 11 gives the Fourier power and average marginal spectrum for the latter half of 1995. The largest peak occurs at 100 h and is due to the dominance of baroclinic instability—the instability of the prevailing atmospheric westerlies that creates cyclones and anticyclones. It is interesting to note that conventional Fourier analysis detected the atmospheric tides.

Figure 12 is the Hilbert spectrum for the final quarter of 1995. Overall, the amplitudes increase with time due to the onset of winter. Using the daily weather maps from 1200 UTC published by the National Oceanic and Atmospheric Administration (NOAA), each maximum was easily correlated with the nearby passage of a cyclone and its associated front; these maxima have been labeled A–F in Fig. 12. For example, maximum A corresponds to the passage of the remnants of Hurricane Opal on 6 October 1995. The passage of a particularly strong cold front on 11 November 1995 is highlighted with the letter G.

Because these data have a high temporal resolution, one would hope to see mesoscale signals as well as synoptic events. To this end, Fig. 13 shows the fifth and eighth IMFs as a function of time (19–29 October 1995), while the original data is plotted on top. Turning to the fifth IMF, many of the peaks could be paired with meteorological events such as the passage of a cold front (cf), a warm front (wf), and trough (t). There are probably other mesoscale events present in this analysis, but

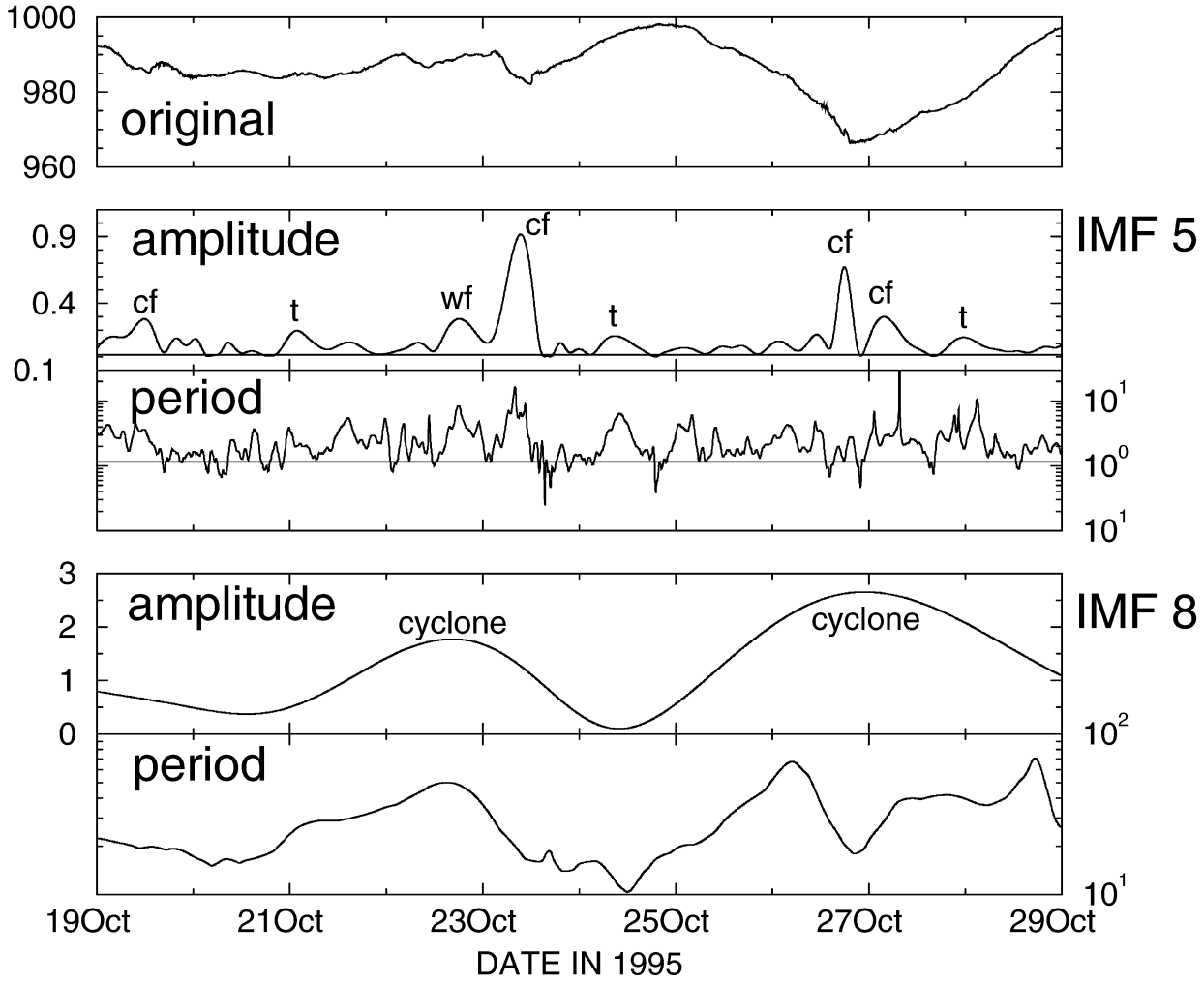

FIG. 13. The fifth and eighth IMFs from the Hilbert–Huang analysis of surface pressure measurements over central Illinois during the 10 days from 19 to 29 Oct 1995. For the IMFs, the scale for the amplitudes (in hPa) is given on the left, while the period (in h) is given on the right.

the lack of other independent data precludes their classification. The eighth IMF clearly shows the passage of two major cyclones during this period. Taken together, Figs. 12 and 13 show how well the Hilbert–Huang transform can discern various mesoscale and synoptic events.

Finally, Fig. 14 shows the Morlet wavelet analysis of the same pressure observations used earlier. The strong signal at ~500 h is associated with the transition from the summer regime to winter. The wavelet analysis agrees with the Hilbert–Huang analysis except that it fails to pick out the individual cyclones and corresponding frontal passages that the Hilbert–Huang transform captures.

4. Conclusions

The purpose of data analysis is to discover the physical processes underlying the observations. For generations scientists have only had Fourier analysis. As our analysis has shown, this technique is quite good for periodic signals, such as atmospheric and oceanic tides. However, it is inadequate for most meteorological signals because they are nonlinear and aperiodic.

Recently several new techniques (short-time Fourier transforms, wavelets, and EOFs) have been developed to handle these aperiodic and nonlinear signals. To this list we now add the promising technique commonly known as Hilbert–Huang transforms because it is adaptive, local, complete, and nearly orthogonal in the sense of Reynolds decomposition $\overline{[f(t) - \overline{f}(t)] \cdot \overline{f}t)} = 0$, where the overbar denotes a local average [see Huang et al. 1998a, their Eq. (6.1)].

The procedure for computing a Hilbert–Huang transform consists of two steps. First, the data are sifted and decomposed into a set of intrinsic mode functions. If the data consisted of a pure sine wave, then its first (and

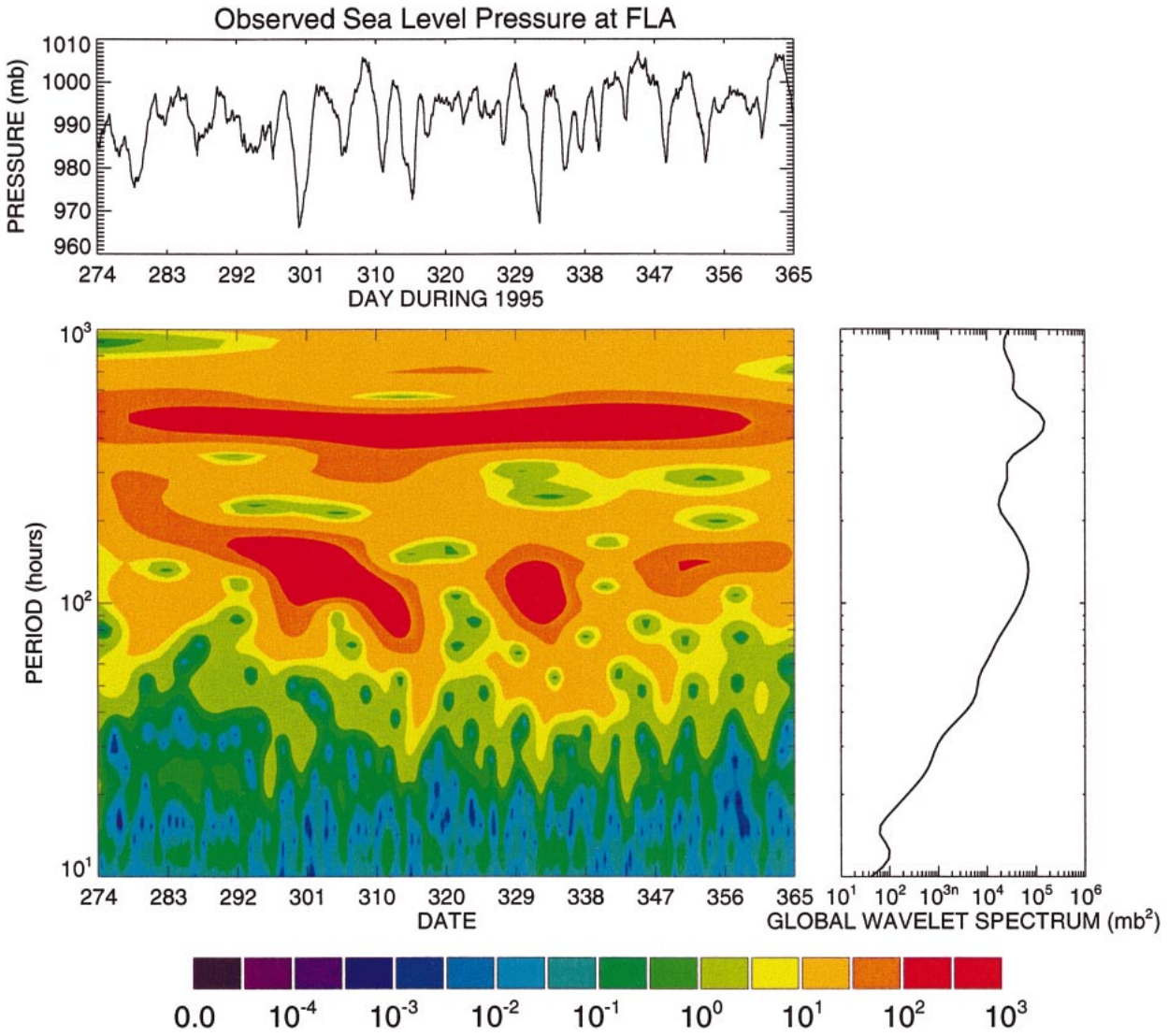

FIG. 14. Morlet wavelet analysis derived from barographic observations near Champaign–Urbana, IL, during the last quarter of 1995.

only) IMF would be the original sine wave. The second step consists of taking the Hilbert transform of each IMF and then computing the instantaneous amplitude and frequency. In the case of a pure sine wave, the Hilbert transform would be a negative cosine and both the instantaneous amplitude and frequency would be constant.

So far this technique has only been applied to climatological datasets. Here the method was tested on datasets that also contain synoptic signals: sea level heights, incoming solar radiation, and barographic observations. These tests showed that the Hilbert–Huang transforms capture a wide variety of phenomena: the diurnal cycle, frontal passages, baroclinic instability, and the seasonal cycle. Therefore, we can use this technique to flag important weather events from floods to ENSO events.

In this paper two methods for presenting Hilbert–Huang transforms are highlighted. One method plots the instantaneous amplitude as a function of time and (instantaneous) period or frequency via the Hilbert spectrum. These plots are useful in suggesting the location and nature of significant events in the original data. Unfortunately, a significance test has not yet been developed for the Hilbert–Huang transform. The second method is the marginal spectrum. It is similar to the popular concept of power spectrum in Fourier analysis and gives a global picture of the dataset.

Acknowledgments. The author would like to gratefully acknowledge Dr. N. E. Huang for allowing the use of his technique and providing considerable insight into the mechanics of how it works. The barographic data were kindly provided by Dr. Stefano Grivet-Talocia.

This paper was greatly improved by suggestions from Dr. David O. Starr and two anonymous reviewers.

REFERENCES

Allen, J. B., and L. R. Rabiner, 1977: A unified approach to short-time Fourier spectrum analysis and synthesis. *Proc. IEEE,* **65,** 1558–1564.

Barnes, A. E., 1992: The calculation of instantaneous frequency and instantaneous bandwidth. *Geophysics,* **57,** 1520–1524.

Čížek, V., 1970: Discrete Hilbert transform. *IEEE Trans. Audio Electroacoust.,* **18,** 340–343.

Czerwinski, R. N., and D. L. Jones, 1997: Adaptive short-time Fourier analysis. *IEEE Signal Process. Lett.,* **4,** 42–45.

Daubechies, I., 1992: *Ten Lectures on Wavelets.* CBMS-NSF Series in Applied Mathematics, Vol. 61. SIAM, 357 pp.

Gabor, D., 1946: Theory of communications. *J. IEE,* **93,** 429–457.

Ghil, M., and Coauthors, 2002: Advanced spectral methods for climatic time series. *Rev. Geophys.,* **40,** 1001, doi:10.1029/2000RG00092.

Grivet-Talocia, S., F. Einaudi, W. L. Clark, R. D. Dennett, G. D. Nastrom, and T. E. VanZandt, 1999: A 4-yr climatology of pressure disturbances using a barometer network in central Illinois. *Mon. Wea. Rev.,* **127,** 1613–1629.

Henrici, P., 1986: *Discrete Fourier Analysis-Cauchy Integrals-Construction of Conformal Maps-Univalent Functions. Vol. 3, Applied and Computational Complex Analysis.* John Wiley and Sons, 637 pp.

Herrmann, E., 1996: On the convolution type kernel regression estimator. Preprints 1833, Dept. of Mathematics, Technical University of Darmstadt, 31 pp. [Available online at http://wwwbib.mathematik.tu-darmstadt.de/Math-Net/Preprints/Listen/shadow/pp1833.html.]

Huang, N. E., and Coauthors, 1998a: The empirical mode decomposition and the Hilbert spectrum for nonlinear and non-stationary time series analysis. *Proc. Roy. Soc. London,* **454A,** 903–995.

——, C. C. Chern, K. Huang, L. W. Salvino, S. R. Long, and K. L. Fan, 2001: A new spectral representation of earthquake data: Hilbert spectral analysis of Station TCU129, Chi-Chi, Taiwan, 21 September 1999. *Bull. Seismol. Soc. Amer.,* **91,** 1310–1338.

Huang, W., Z. Shen, N. E. Huang, and Y. C. Fung, 1998b: Use of intrinsic modes in biology: Examples of indicial response of pulmonary blood pressure to ± step hypoxia. *Proc. Natl. Acad. Sci. USA,* **95,** 12 766–12 771.

Koch, D. M., and M. E. Mann, 1996: Spatial and temporal variability of ^{7}Be surface concentrations. *Tellus,* **48B,** 387–396.

Komm, R. W., F. Hill, and R. Howe, 2001: Empirical mode decomposition and Hilbert analysis applied to rotation residuals of the solar convection zone. *Astrophys. J.,* **558,** 428–441.

Pan, J.-Y., X.-H. Yan, Q.-N. Zheng, W. T. Liu, and V. V. Klemas, 2003: Interpretation of scatterometer ocean surface wind vector EOFs over the Northwestern Pacific. *Remote Sens. Environ.,* **84,** 53–68.

Ryan, T. P., 1997: *Modern Regression Methods.* John Wiley and Sons, 515 pp.

Salisbury, J. I., and M. Wimbush, 2002: Using modern time series analysis techniques to predict ENSO events from the SOI time series. *Nonlinear Process. Geophys.,* **9,** 341–345.

Shapiro, R., 1970: Smoothing, filtering, and boundary effects. *Rev. Geophys. Space Phys.,* **8,** 359–387.

Susanto, R. D., A. L. Gordon, J. Sprintall, and B. Herunadi, 2000: Intraseasonal variability and tides in Makassar Strait. *Geophys. Res. Lett.,* **27,** 1499–1502.

Torrence, C., and G. P. Compo, 1998: A practical guide to wavelet analysis. *Bull. Amer. Meteor. Soc.,* **79,** 61–78.

Wu, M.-L. C., S. Schubert, and N. E. Huang, 1999: The development of the South Asian summer monsoon and the intraseasonal oscillation. *J. Climate,* **12,** 2054–2075.

Xie, L., L. J. Pietrafesa, and K. J. Wu, 2002: Interannual and decadal variability of land-falling tropical cyclones in the southeast coastal states of the United States. *Adv. Atmos. Sci.,* **19,** 677–686.